Korean J. Chem. Eng., 34(8), 2147-2153 (2017)
DOI: 10.1007/s11814-017-0120-3

pISSN: 0256-1115
eISSN: 1975-7220

Porous MnO_2/CNT catalysts with a large specific surface area for the decomposition of hydrogen peroxide

Min June Kim*, Kang-Bong Lee, Myung-gi Seo*,†, and Kwan-Young Lee*,***,†**

*Department of Chemical and Biological Engineering, Korea University, 145 Anam-ro, Seoul 02841, Korea
**Advanced Analysis Center and Green City Technology Institute, Korea Institute of Science & Technology, Seoul 02792, Korea
***Green School, Korea University, 145 Anam-ro, Seoul 02841, Korea
(*Received 21 December 2016 • accepted 25 April 2017*)

Abstract−H_2O_2 vapor sterilization is an effective and safe method for removing various pathogens. To improve the efficiency of this technique, the time required for sterilization must be shortened. The aeration time constitutes a large portion of the total sterilization time; therefore, the development of a catalyst for H_2O_2 decomposition is necessary. Bulk MnO_2 is typically used in H_2O_2 decomposition, but it has a low specific surface area. To increase H_2O_2 decomposition activity, specific surface area and electron transfer ability of catalyst need improvement. In this study, MnO_2/CNT(x), where x denotes the weight ratio of CTAB to H_2O in the catalyst preparation, was synthesized using a soft template method with varying amounts of the template. Overall, the catalyst specific surface area remarkably increased to 190-200 m^2/g from 0.043 m^2/g for bulk MnO_2 and these increased surface areas resulted in superior H_2O_2 decomposition activity. Among the CNT-supported catalysts tested, MnO_2/CNT (1.0) exhibited the highest activity, which was 570 times that of bulk MnO_2. Aeration times were also calculated with some assumptions and the aeration can be finished within 1 hr (bulk MnO_2 needs about 25 hr).

Keywords: Manganese Oxide Catalyst, Soft Template Method, Large Surface Area, Hydrogen Peroxide Decomposition, Aeration

INTRODUCTION

Development of effective sterilization techniques has recently attracted attention due to the outbreak of devastating infectious diseases and development of biochemical weapons, such as anthrax bacillus. For example, the recent Middle East respiratory syndrome (MERS) outbreak in 2012 brought 1,728 infections and 624 deaths by 2016 [1]. Although many types of pathogens can be transmitted between people through a variety of pathways, many of the infected and deceased were infected after admission to a hospital in which other patients diagnosed with MERS were being treated. Therefore, sterilization of hospital beds, equipment, tools, rooms and other spaces is crucial to prevent nosocomial transmission. Depending on the applications, sterilization methods involve the use of heat [2], chemicals [3], irradiation [4], or high pressure [5] to remove these viruses and bacteria. In particular, chemical sterilization is appropriate for application to larger spaces, such as hospital rooms. Ethylene oxide (EO) is a representative sterilant that is used for chemical sterilization. EO sterilization has a mild operating temperature that ranges from 49 °C to 63 °C [6], and therefore, this approach is primarily used when the materials that need to be sterilized cannot withstand heat. However, time weighted average (TWA), which is a measure of the permissible exposure limit, of ethylene oxide is 0.1 ppm. This legal limit was set because a longer exposure to a higher amount may induce cancer or genetic damage [7]. The use of hydrogen peroxide as a sterilant offers advantages related safety compared to ethylene oxide because its TWA is 1 ppm. Hydrogen peroxide sterilization has been used as an effective method, and Bioquell is a representative company that provides hydrogen peroxide vapor sterilization equipment.

The hydrogen peroxide sterilization cycle consists of evaporation, dwell and aeration steps. Vaporized hydrogen peroxide can remove pathogens over a large space within a short time. During aeration, the hydrogen peroxide concentration is reduced below its toxic threshold. To improve the operational efficiency of the hydrogen peroxide vapor sterilization equipment, the run time of the equipment must be reduced, especially that of the aeration step because it accounts for more than 50% of the total time [8]. To reduce the aeration time, the development of an active catalyst for hydrogen peroxide decomposition is necessary because adjusting only the air condition is restrictive due to the safe hydrogen peroxide concentration level being 1 ppm [9], which is very low. In addition, the catalyst must exhibit excellent decomposition activity because the amount of catalyst that is used is limited in the sterilization machine.

Hydrogen peroxide can be decomposed by various precious metals (e.g., Pd and Pt [10-14]) or transition metal oxides (e.g., MnO_2 [15], Fe_2O_3 [16] and Al-La-Mn oxide [17]) and perovskite [18]. Recently, metal-Schiff base complexes (e.g., Mn_2A, A=3,5-bis[(2-hydroxy-40-sodiumsulphatoehtyl sulphonyl)azobenzene-methy-

†To whom correspondence should be addressed.
E-mail: kylee@korea.ac.kr, bluebird18@korea.ac.kr
‡This article is dedicated to Prof. Ki-Pung Yoo on the occasion of his retirement from Sogang University.

neimino]-benzoic acid) have been reported as the catalysts with a high H_2O_2 decomposition activity [19,20]. However, precious metals are expensive, and metal-Schiff base catalyst synthesis has several drawbacks, including a long synthesis time and the use of a hazardous organic solvent. Therefore, transition metal oxides as heterogeneous catalysts for hydrogen peroxide decomposition are attractive materials.

Hydrogen peroxide decomposition via transition metal oxides is based on redox catalysis, and the corresponding reaction mechanism is as follows [21]:

$$M^{(n)+}+H_2O_2 \rightarrow M^{(n+1)+}+OH^-+OH\cdot$$
$$OH\cdot+H_2O_2 \rightarrow H_2O+HO_2\cdot$$
$$HO_2\cdot+M^{(n+1)+} \rightarrow M^{(n)+}+H^++O_2$$

(M: transition metal, ·: radical)

H_2O_2 exchanges an electron with $M^{(n)+}$ and decomposes into OH^- and OH·, and finally into H_2O and O_2. According to this mechanism, the electron transfer ability of catalyst is expected as a factor of H_2O_2 decomposition.

Nonprecious metal catalysts have been used in various catalytic reactions due to being inexpensive [22-24]. Manganese oxide is also used as a catalyst for various reactions [25-29] and exhibits a high H_2O_2 decomposition activity, resulting from facile reversible changes in its oxidation state. However, the commercially available MnO_2 catalyst has a low specific surface area that is less than 10 m^2/g [30], and many studies have focused on increasing the surface area of catalysts. A porous catalyst structure is commonly studied, and a porous transition metal oxide may also be possible. Many of the porous MnO_2 structures exhibited improvements over the bulk MnO_2 regarding the catalytic reactions such as the HCHO de- composition [31], the H_2O_2 decomposition [32], and the reaction in the electrical capacitor [33,34].

In this study, we synthesized porous MnO_2/carbon nanotube (CNT), using a soft template method, that has a large specific surface area of MnO_2, which was related to the porous structure and thin layer of MnO_2 on the CNT. In addition, the conductive carbon materials (e.g., CNT and graphene) enhance the electron transferability of catalyst [35]. The porous oxide on CNT can be achieved using the soft template method with appropriate organic surfactants [35-37]. The soft template method provides a facile synthesis method for porous materials due to its mild conditions in the absence of a hydrothermal treatment and calcination. To determine the effect of the template amount on the catalytic properties, the CTAB amount was varied during the catalyst synthesis.

EXPERIMENTAL

1. Materials

Absolute ethanol (C_2H_5OH, 99.5%, Sigma-Aldrich), ammonium nitrate (NH_4NO_3, 98%, Sigma-Aldrich), multi-wall carbon nanotube (CNT, 98%, Sigma-Aldrich), cetyltrimethyl ammonium bromide (CTAB, 98%, Sigma-Aldrich), hydrogen peroxide (H_2O_2, 35 wt% in H_2O, Sigma-Aldrich), sulfuric acid solution (H_2SO_4, 0.1 N, Fluka), manganese dioxide (MnO_2, 99%, Sigma-Aldrich), potassium permanganate ($KMnO_4$, 99%, Sigma-Aldrich), potassium iodide solution (KI, 0.1 N, Samchun), and sodium thiosulfate solution ($Na_2S_2O_3$, 0.1 N, Fluka) were used without further purification.

2. Catalyst Preparation

Porous MnO_2/CNT was synthesized using a soft template method based on a previously reported [35]. Scheme 1 shows the catalyst preparation process, which is composed of the following steps: (1) hydrophobic interaction of CTA^+ with CNT, (2) electrostatic interaction of MnO_4^- with CTA^+ and self-assembly of MnO_4^-/CTA^+/CNT, (3) MnO_4^- reduction to MnO_2 via ethanol addition, and (4) template removal using ion exchange. Details of the procedure are provided below. First, CTAB (0.6 g, 0.8 g, 1 g, 1.2 g) was dissolved in 90 mL of DI water, and 70 mg of CNT was added to the solution. The mixture was sonicated for 4 h, and then 10 mL of a $KMnO_4$ solution (0.1 M) was added before stirring for 1 h. In this step, MnO_4^- ions were attached to CTA^+ which had formed layer on CNT via electrostatic interactions. Finally, 40 mL of absolute ethanol was added to reduce permanganate to manganese oxide, and the

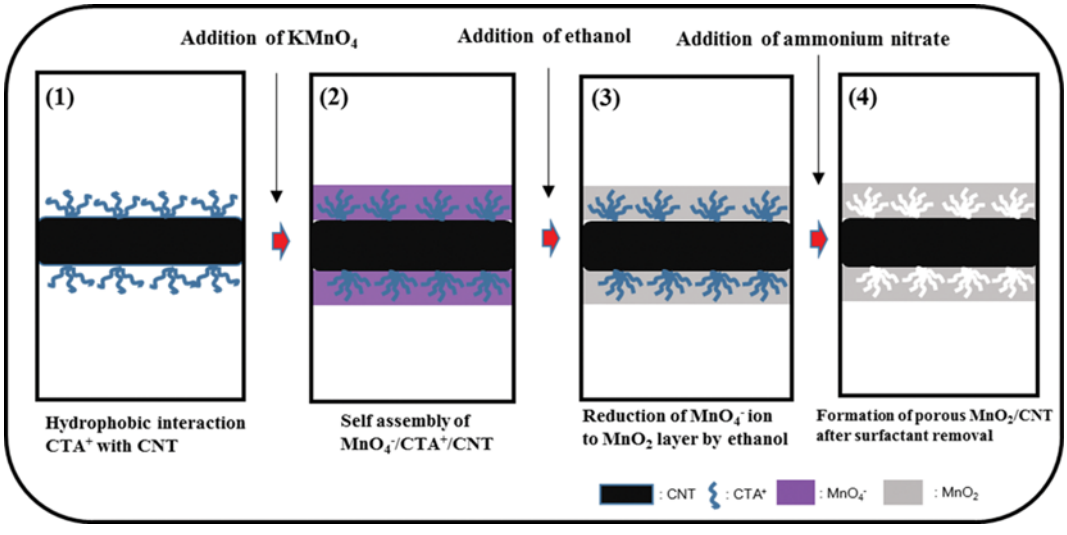

Scheme 1. MnO_2/CNT preparation process.

mixture was stirred for 12 h. The catalysts were filtered and washed with ethanol. The recovered products were dried overnight at 80 °C. To achieve a porous structure, CTAB was removed via ion exchange with ammonium nitrate. The catalyst was dispersed in an ethanol solution for which the ammonium nitrate was dissolved, followed by stirring for 30 min at 60 °C. Similar to previous recovery processes, the catalysts were filtered and washed. The CTAB/water solvent weight ratios are denoted as x in MnO_2/CNT (x) (x=0.6, 0.8, 1.0, 1.2).

3. Characterization

Using a BELSORP-max (BEL Japan Inc. Osaka, Japan), nitrogen adsorption-desorption isotherms of MnO_2/CNT were measured. The specific surface areas of the catalysts were calculated using the Brunauer-Emmett-Teller (BET) equation. The degassing conditions were 100 °C and 6 hr under reduced pressure.

To measure the mass fraction of MnO_2 in the catalysts, inductively coupled plasma optical emission spectroscopy (ICP-OES) was performed using a JY Ultima2C (Jobin Yvon, France) dual ICP-OES spectrometer. The samples were pretreated by dissolution in a mixture consisting of aqua regia and hydrofluoric acid. The analysis was carried out at 200 °C under reduced pressure, provided by the Korean Basic Science Institute (KBSI).

X-ray diffraction (XRD) was performed to investigate the structure of MnO_2/CNT using a D8 Advanced LynxEye (Bruker). The scanning speed was 2°/min, and the scanning range was 10° to 90°. The beam source was Cu-Kα irradiation (α=1.5406 Å).

Scanning transmission electron microscopy (STEM) images of MnO_2/CNT were obtained to identify the structure of the composite using a Tecnai G^2 11 F30 instrument (FEI Company, OR, USA). The catalysts were dispersed in ethanol and sampled on a Cu grid. To identify the Mn element in the catalyst structure, energy-dispersive X-ray (EDX) spectroscopy was also performed.

To measure the Mn electronic state, X-ray photoelectron spectroscopy (XPS) was performed on an ESCA2000 (VG microtech: U.K.). The operating conditions were 10^{-10} Torr with an AlKa X-ray anode source.

4. Hydrogen Peroxide Decomposition

The decomposition of hydrogen peroxide was in a 200 mL double jacket glass reactor. The initial concentration of H_2O_2 was set to 1,000 ppm by diluting 35 wt% H_2O_2 in 100 mL of DI water. 10 mg of each catalyst was added to the reaction solvent and stirred with a magnetic stirrer (1,200 rpm). The reaction temperature was maintained at 25 °C using a circulator. To examine the time progression of the change in the H_2O_2 concentration, we sampled the solution three times at an interval of 10 min. The concentration was measured via iodide titration. To compare the H_2O_2 decomposition activity, the hydrogen peroxide decomposition was also performed using bulk MnO_2 (Sigma Aldrich, 200 mg), and the other reaction conditions remained the same as those employed for MnO_2/CNT. To compare the activation energies of the MnO_2/CNT (1.0) and the bulk MnO_2, the H_2O_2 decomposition reactions were carried out at 15 °C and 35 °C additionally. Subsequently, the activation energy of each catalyst was obtained from the slope of linear line on the Arrhenius plot.

5. Iodide Titration

The H_2O_2 concentration in the reaction was measured via iodide titration [38]. The process follows two chemical reactions. First, 5 mL of a KI solution (0.1 N) and 5 mL of a H_2SO_4 solution (0.1 N) were added to a vial. Drops of an ammonium molybdate solution were used as a catalyst for iodide oxidation, and a starch solution (0.5 wt%) was used as an indicator, which turned indigo color by reacting with I_2 (Eq. (1)). The sampled reaction solution from the reactor was added, and a certain amount of I_2 was formed as a function of the H_2O_2 amount. The indigo solution was titrated with the sodium thiosulfate solution (Fluka) until the solution was colorless (Eq. (2)). Using Eq. (3), we calculated the hydrogen peroxide concentration.

$$H_2O_2 + 2\,KI + H_2SO_4 \rightarrow I_2 + K_2SO_4 + 2\,H_2O \quad (1)$$

$$I_2 + 2\,Na_2S_2O_3 \rightarrow Na_2S_4O_6 + 2\,NaI \quad (2)$$

$$H_2O_2\ (wt\%) = \frac{17.007 \times 0.01 \times A}{B \times 1000} \quad (3)$$

A=volume of $Na_2S_2O_3$ (μL), B=weight of sampled solution (g)

6. Hydrogen Peroxide Reaction Rate Constant Calculation

Hydrogen peroxide decomposes into water and oxygen (Eq. (4)), and the reaction follows pseudo first-order kinetics [39,40] as expressed by Eq. (5).

$$H_2O_2 \xrightarrow{k_d} H_2O + 1/2\ O_2 \quad (4)$$

$$\ln\left(\frac{[H_2O_2]}{[H_2O_2]_0}\right) = k_d t,\ \ k_d = k_{MnO_2} \times MnO_2\ \text{weight (g)} \quad (5)$$

(k_d: reaction rate constant, k_{MnO_2}: reaction rate constant per MnO_2 weight)

The reaction constants (k_{MnO_2}) of the catalysts were compared to measure the hydrogen peroxide decomposition activity.

7. Aeration Time Calculation

Aeration times ($t_{aeration}$) were calculated in a 75 m^3 room and at an initial concentration of 1,000 ppm to a final concentration of 1 ppm. The overall process and assumptions made for this calculation are detailed in supplementary material.

RESULTS AND DISCUSSION

Fig. 1 shows the STEM images of CNT and MnO_2/CNT (1.0) before and after CTAB removal. A bare CNT has a thickness of approximately 10-12 nm, as shown in Fig. 1(a), and MnO_2/CNT (1.0) before CTAB removal has a thickness of approximately 20 nm, as shown in Fig. 1(b), which corresponds to Scheme 1-(3). Based on the STEM images, a thin layer of MnO_2 was deposited on CNT. The MnO_2/CNT structure is a long CNT tube uniformly surrounded by a layer of MnO_2 (bright color). Based on STEM-EDX mapping shown (Fig. 1(d)), the MnO_2 layer was uniformly deposited along the CNT structure. After CTAB removal, the MnO_2 layers were partially irregular on the CNT, as shown in Fig. 1(c), corresponding to Scheme 1-(4). In Fig. 2(a), (b), and (c), the MnO_2/CNT catalysts exhibited a similar structure with MnO_2/CNT (1.0). On the other hand, the particle size of bulk MnO_2 was in the 200-300 nm range (Fig. 2(d)).

Fig. 3 shows the XRD patterns for MnO_2/CNT and bulk MnO_2.

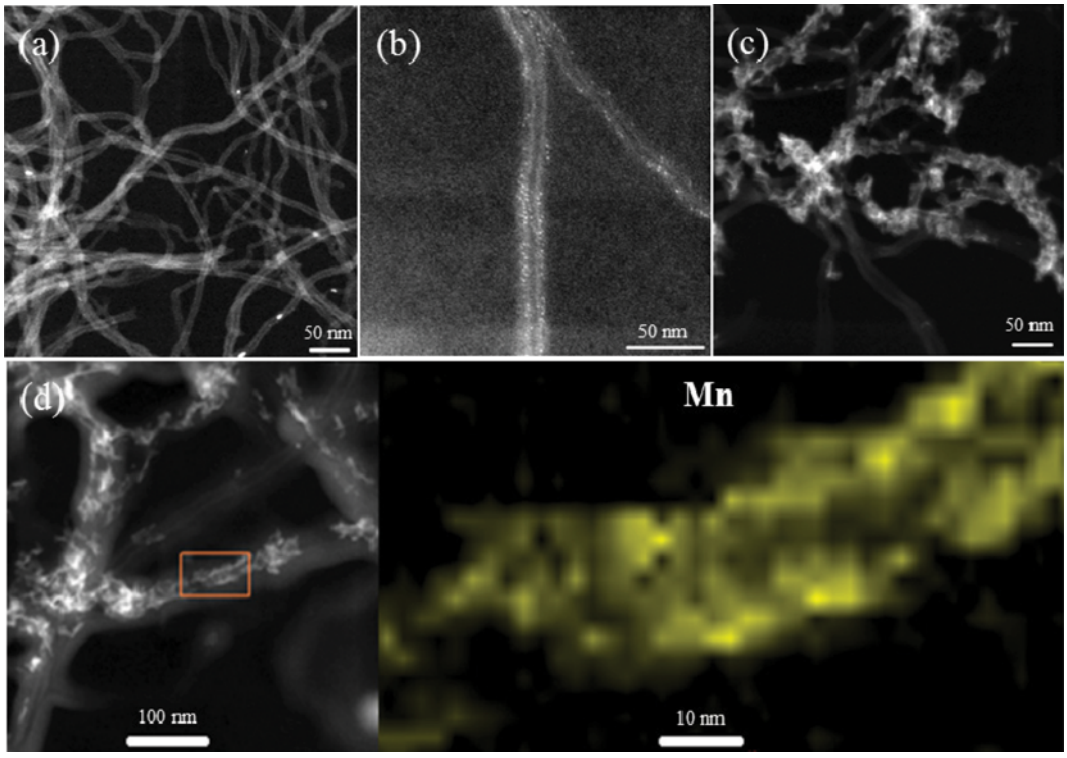

Fig. 1. STEM images of (a) CNT, (b) MnO_2/CNT (1.0) (before CTAB removal), (c) MnO_2/CNT (1.0) (after CTAB removal) and (d) STEM EDX of MnO_2/CNT (1.0).

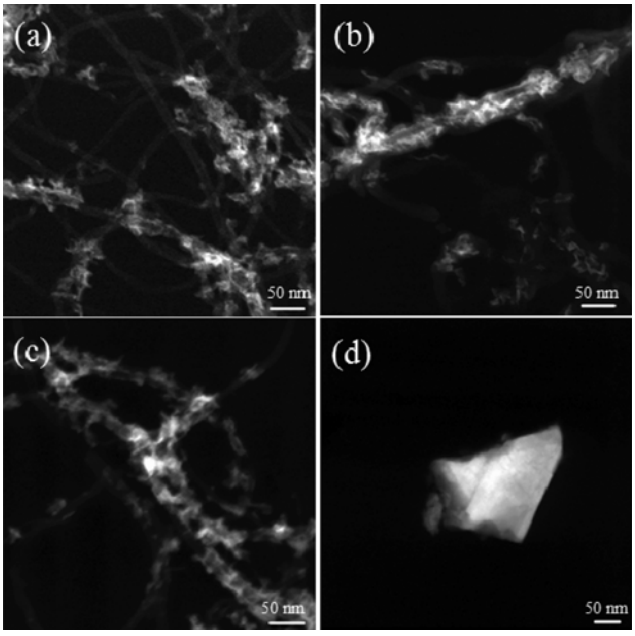

Fig. 2. STEM images of (a) MnO_2/CNT (0.6), (b) MnO_2/CNT (0.8), (c) MnO_2/CNT (1.2) and (d) bulk MnO_2 (Sigma-Aldrich).

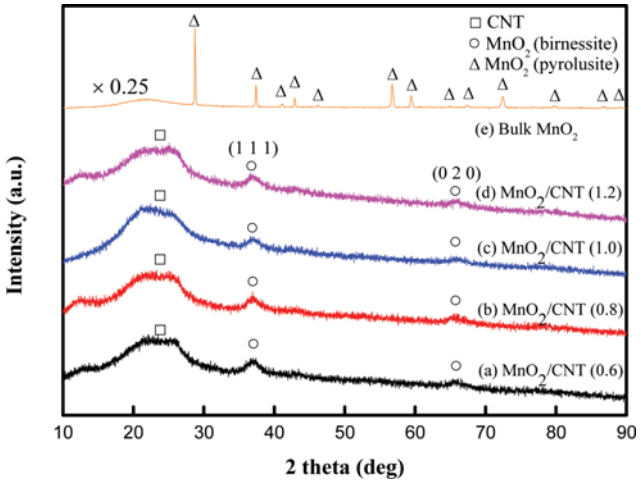

Fig. 3. XRD patterns of the catalysts: (a) MnO_2/CNT (0.6), (b) MnO_2/CNT (0.8), (c) MnO_2/CNT (1.0), (d) MnO_2/CNT (1.2) and (e) bulk MnO_2 (Sigma).

In XRD results of MnO_2/CNT contained three broad peaks at two theta values of 26°, 37°, and 66°. The 26° peak corresponds to the (0 0 2) facet of the CNT structure [41], and the 37° and 66° peaks were due to the (1 1 1) and (0 2 0) facets, respectively, of the manganese oxide monoclinic structure, which was formed by reducing $KMnO_4$ with ethanol (JCPDS 42-1317). These broad peaks indicate that the MnO_2 layer deposited on the CNT in all of the catalysts had low crystallinity. Using the XRD results, the crystallite size of MnO_2 was calculated with the Scherrer equation. In Table 1, the crystallite sizes of MnO_2 in the synthesized catalysts ranged from 3.4 nm to 4.4 nm, and these values increased as the CTAB template amount decreased. Another study also reported a decrease in the crystallite size of the catalyst as the template amount increased [42]. The bulk MnO_2 (Sigma-Aldrich) crystallite size was approxi-

Table 1. Crystallite sizes of the catalysts

Catalyst	Crystallite size (nm)[a]
MnO_2/CNT (0.6)	4.4
MnO_2/CNT (0.8)	4.1
MnO_2/CNT (1.0)	3.7
MnO_2/CNT (1.2)	3.4

[a]Crystallite size of the catalyst was calculated from the XRD data

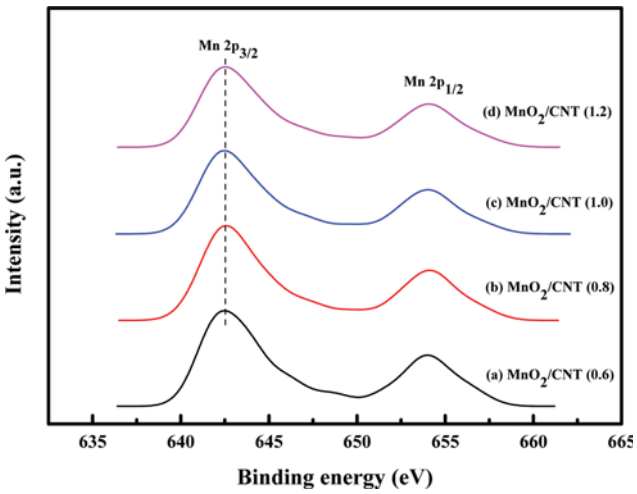

Fig. 4. Mn 2p XPS of the synthesized catalysts.

mately 100 nm, which was calculated using the Scherrer equation, and the specific surface area of MnO_2/CNT is expected to be much larger than that of bulk MnO_2.

Fig. 4 shows the Mn electronic states of the synthesized catalysts. The oxidation states of the Mn element in the metal oxide are varied, and the binding energies of Mn^{2+}, Mn^{3+}, and Mn^{4+} appear in the region from 640 eV to 643 eV in the Mn $2p_{3/2}$ XPS spectra [43]. The MnO_2/CNT catalysts showed similar binding

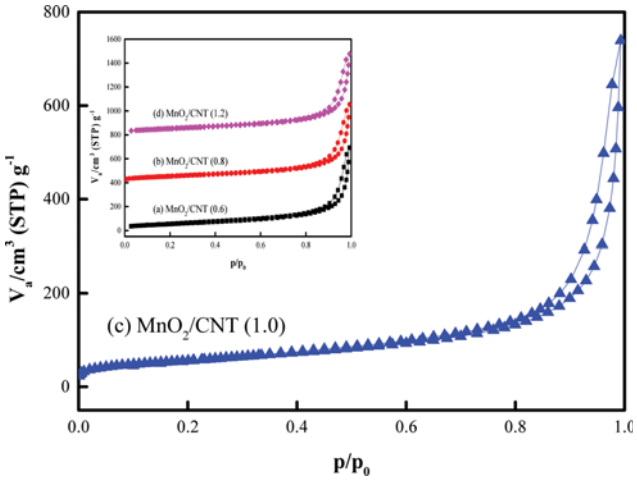

Fig. 5. N_2 adsorption-desorption isotherms of the catalysts: (a) MnO_2/CNT (0.6), (b) MnO_2/CNT (0.8), (c) MnO_2/CNT (1.0) and (d) MnO_2/CNT (1.2).

Table 2. Specific surface areas, Mn content and MnO_2 weights of the catalysts

Catalyst	Specific surface area (m^2/g)[a]	Mn (wt%)[b]	MnO_2 (wt%)[c]
MnO_2/CNT (0.6)	197.7	31.1	49.2
MnO_2/CNT (0.8)	194.2	30.7	48.6
MnO_2/CNT (1.0)	200.6	29.4	46.5
MnO_2/CNT (1.2)	190.5	32.2	50.9
Bulk MnO_2	0.043	-	100

[a]Specific surface area of the catalyst was calculated from the BET equation
[b]Mn weight (%) was confirmed by ICP-OES
[c]MnO_2 weight (%) was calculated from the Mn weight (%) assuming that the Mn composition corresponded to MnO_2 in the catalysts

energies in the XPS spectra, which are confirmed by the dashed line in Fig. 4, where the Mn electronic states are nearly the same as those in the synthesized catalysts.

Fig. 5 shows the N_2 adsorption-desorption isotherms of the MnO_2/CNT catalysts. At an approximately near-zero relative pressure, a slight increase in the monolayer adsorption of N_2 on the catalyst was observed. The adsorption amount gradually increased in the region from p/p_0 of 0.1 to a p/p_0 of 0.8, and a sharp increase, which may have resulted from the interparticle void space that is due to the catalyst packing, which appeared in the region from a p/p_0 of 0.8 to a p/p_0 of 1.0. Based on these results, the adsorption isotherm can be regarded as Type II [44]. Additionally, a hysteresis loop is present in the isotherm through a wide region (p/p_0 0.4 to p/p_0 1.0). The hysteresis under the low pressure seems to be due to the porous structure that is formed by the removal of the CTAB, while the hysteresis under the high pressure appeared to be due to the CNT's entangled structure.

Table 2 lists the specific surface areas, which were calculated from the BET equation and Mn content, which was obtained from ICP-OES analysis. The Mn content ranged from 29.4 wt% to 32.2 wt%, about 30 wt%. The MnO_2/CNT catalysts exhibited much larger specific surface areas (190-200 m^2/g) than bulk MnO_2 (0.043 m^2/g). These large surface areas resulted from the formation of a very thin layer of MnO_2 on the CNT, as confirmed in Fig. 1, and the porous structure of the MnO_2 formed during the CTAB removal. In addition, the specific surface area of the catalysts varied when only the CTAB amount was changed, and the other material quantities were held constant. The largest specific surface area was observed for MnO_2/CNT (1.0).

The reaction rate constant (k_d) was obtained from the slope of the linear line in Fig. 6, and k_{MnO_2} of the catalysts determined from k_d and MnO_2 weights are shown in Table 3. The MnO_2/CNT catalysts exhibited a 350- to 570-fold improvement in the H_2O_2 decomposition activity (k_{MnO_2}=22.47-35.48 $g^{-1}min^{-1}$) compared to that of bulk MnO_2 (0.0625 $g^{-1}min^{-1}$). This result confirmed that MnO_2/CNT exhibited a significant improvement in the catalytic activity for H_2O_2 decomposition, which originated from the large specific surface area. Aeration times in 75 m^3 (5 m×6 m×2.5 m) system for MnO_2/CNT (1.0) and bulk MnO_2 were 0.89 hr and 25 hr, respec-

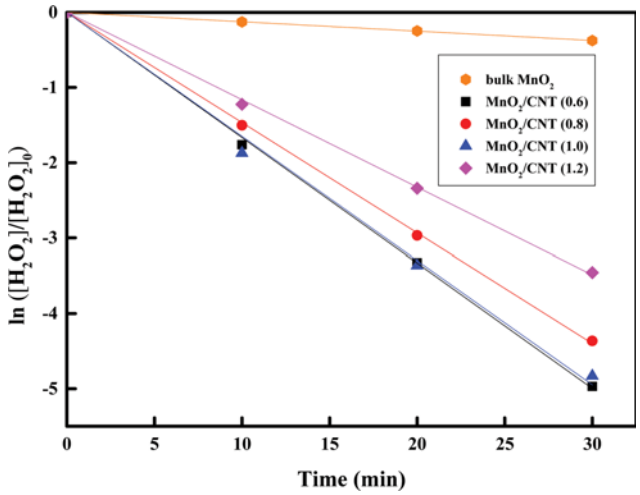

Fig. 6. Hydrogen peroxide decomposition. Test conditions: 25 °C, 1 atm, 10 mg MnO_2/CNT (bulk MnO_2 200 mg), 100 mL water containing $[H_2O_2]_0$ 1,000 ppm, stirring rate 1,200 rpm.

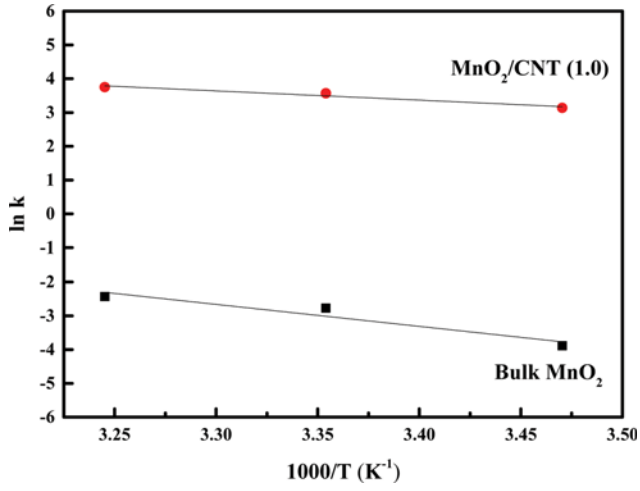

Fig. 7. Arrhenius plot of hydrogen peroxide decomposition.

tively (Supplementary material), which clearly indicates the synthesized catalyst's superior performance for hydrogen peroxide vapor sterilization.

Fig. 7 shows the Arrhenius plots of the MnO_2/CNT (1.0) and the bulk MnO_2. From the plot slopes, the activation energies of each catalyst were calculated, and the MnO_2/CNT activation energy (22.7 kJ/mol) is lower than that of bulk MnO_2 (54.1 kJ/mol). Therefore, the reason that the synthesized catalyst showed the superior

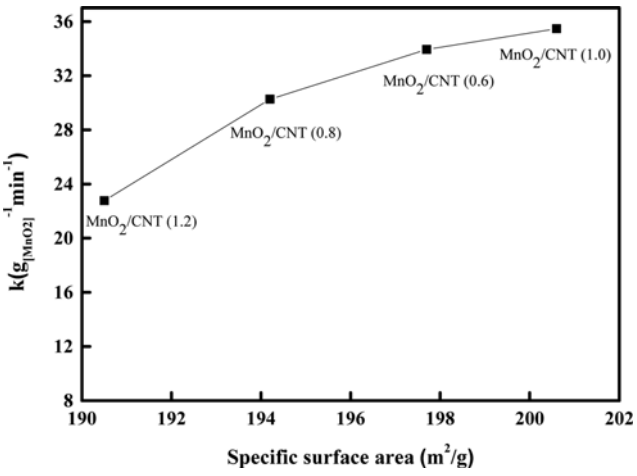

Fig. 8. k_{MnO_2} of the catalysts (hydrogen peroxide decomposition reaction assumed to follow pseudo first-order kinetics).

H_2O_2 decomposition activity is the increase of active sites and the reduction of the activation energy compared with the bulk MnO_2.

Fig. 8 shows a plot k_{MnO_2} of MnO_2/CNT (x). The H_2O_2 decomposition activity is proportional to the specific surface area, which was confirmed by the plot. The difference in CTAB addition amount during catalyst synthesis affected the specific surface area [37] and resulted in changes in the catalytic activity. Although the specific surface area from N_2 adsorption-desorption isotherm analysis does not exactly correspond to the specific surface of MnO_2 in the catalyst, we can assume that the MnO_2 surface area is most likely proportional to the MnO_2/CNT catalyst specific surface area because the MnO_2 layer nearly covers the CNT [35]. Therefore, the H_2O_2 decomposition activity is correlated with the MnO_2 surface area of the catalyst.

CONCLUSIONS

MnO_2/CNT catalysts synthesized using a soft template method exhibited improvement in catalytic activity for hydrogen peroxide decomposition compared to that of bulk MnO_2 due to the increased specific surface area and reduced activation energy in the hydrogen peroxide decomposition. The template amount was varied to determine the optimal mass ratio between the catalyst and the support, and the specific surface area of the catalyst was identified as a factor in determining the catalytic activity. The largest specific surface area was observed for MnO_2/CNT (1.0), which exhibited the highest activity among the synthesized catalysts. In a

Table 3. Reaction rate constants (k_d and k_{MnO_2}) of the catalysts

Catalyst	$[H_2O_2]_0$ (t=0, ppm)	$[H_2O_2]$ (t=30 min, ppm)	k_d (min^{-1})	k_{MnO_2} ($g^{-1}\cdot min^{-1}$)
MnO_2/CNT (0.6)	1065	7.4	0.167	33.94
MnO_2/CNT (0.8)	1100	14	0.147	30.27
MnO_2/CNT (1.0)	1040	8.3	0.165	35.48
MnO_2/CNT (1.2)	1040	32.8	0.116	22.77
Bulk MnO_2	1045	718	0.0125	0.0625

vapor sterilization system, aeration times for bulk MnO_2 (Sigma-Aldrich) and MnO_2/CNT (1.0) were calculated, and the times were shortened from 25 hr (bulk MnO_2) to 0.89 hr (MnO_2/CNT (1.0)). The synthesis is easily carried out in mild conditions without the need for hydrothermal setting and calcination. Therefore, the utilization of MnO_2/CNT as a decomposition catalyst in hydrogen peroxide sterilization provides a good approach for enhancing the efficiency of the hydrogen peroxide sterilization system.

ACKNOWLEDGEMENTS

This research was financially supported by the Korea Institute of Science and Technology (2E26710).

SUPPORTING INFORMATION

Additional information as noted in the text. This information is available via the Internet at http://www.springer.com/chemistry/journal/11814.

REFERENCES

1. E. de Wit, N. van Doremalen, D. Falzarano and V. J. Munster, *Nat. Rev. Microbiol.*, **14**, 523 (2016).
2. R. A. Molins. *Food irradiation: Principles and applications*, Wiley-IEEE, New York (2001).
3. M. J. Alfa, P. DeGagne, N. Olson and R. Hizon, *Am. J. Infect. Control*, **26**, 469 (1998).
4. D. J. Berry, B. H. Currier, M. B. Mayor and J. P. Collier, *Clin. Orthop. Relat. Res.*, **470**, 1805 (2012).
5. A. M. Matser, B. Krebbers, R. W. van den Berg and P. V. Bartels, *Trends Food Sci. Technol.*, **15**, 79 (2004).
6. R. S. King, T. N. C. Devanathan, S. T. Lin, W. L. Rohr and D. F. Swarts, US Patent, 5,522,897 (1995).
7. P. J. Landrigan, T. J. Meinhardt, J. Gordon, J. A. Lipscomb, J. R. Burg, L. F. Mazzuckelli, T. R. Lewis and R. A. Lemen, *Am. J. Ind. Med.*, **6**, 103 (1984).
8. T. Holmdahl, P. Lanbeck, M. Wullt and M. H. Walder, *Infect. Control Hosp. Epidemiol.*, **32**, 831 (2011).
9. G. Mastrangelo, R. Zanibellato, U. Fedeli, E. Fadda and J. H. Lange, *Int. J. Environ. Health Res.*, **15**, 313 (2005).
10. G. Bianchi, F. Mazza and T. Mussini, *Electrochim. Acta*, **7**, 457 (1962).
11. H. E. Jeong, S. Kim, M.-g. Seo, D.-W. Lee and K.-Y. Lee, *J. Mol. Catal. A: Chem.*, **420**, 88 (2016).
12. M.-g. Seo, S. Kim, D.-W. Lee, H. E. Jeong and K.-Y. Lee, *Appl. Catal., A.: Gen.*, **511**, 87 (2016).
13. M.-g. Seo, S. Kim, H. E. Jeong, D.-W. Lee and K.-Y. Lee, *J. Mol. Catal. A: Chem.*, **413**, 1 (2016).
14. M.-g. Seo, H. J. Kim, S. S. Han and K.-Y. Lee, *Catal. Surv. Asia*, **21**, 1 (2017).
15. M. A. Hasan, M. I. Zaki, L. Pasupulety and K. Kumari, *Appl. Catal., A.: Gen.*, **181**, 171 (1999).
16. M. Hermanek, R. Zboril, I. Medrik, J. Pechousek and C. Gregor, *J. Am. Chem. Soc.*, **129**, 10929 (2007).
17. G. Kim, K. Y. Jung, C.-H. Lee, J.-S. Han, B.-H. Jeong, Y.-K. Park and J.-K. Jeon, *Mater. Res. Bull.*, **82**, 76 (2016).
18. Y. N. Lee, R. M. Lago, J. L. G. Fierro and J. González, *Appl. Catal., A.: Gen.*, **215**, 245 (2001).
19. K. C. Gupta, H. K. Abdulkadir and S. Chand, *J. Mol. Catal. A: Chem.*, **202**, 253 (2003).
20. K. Zhang, C. Zhang and K. Xie, *Text. Res. J.*, **85**, 1704 (2015).
21. C. Walling and A. Goosen, *J. Am. Chem. Soc.*, **95**, 2987 (1973).
22. D.-W. Lee, M. S. Lee, J. Y. Lee, S. Kim, H.-J. Eom, D. J. Moon and K.-Y. Lee, *Catal. Today*, **210**, 2 (2013).
23. S.-C. Baek, J.-W. Bae, J. Y. Cheon, K.-W. Jun and K.-Y. Lee, *Catal. Lett.*, **141**, 224 (2011).
24. J.-H. Ryu, K.-Y. Lee, H. La, H.-J. Kim, J.-I. Yang and H. Jung, *J. Power Sources*, **171**, 499 (2007).
25. T. Wang, X. Zhang, H. Liu, Y. Guo, Y. Zhang, Y. Wang and B. Sun, *Catal. Surv. Asia*, **21**, 94 (2017).
26. S. W. Jeon, J. E. Lee, J. K. Park and S. H. Kim, *Korean J. Chem. Eng.*, **32**, 230 (2015).
27. M. Amini, *Korean J. Chem. Eng.*, **33**, 126 (2016).
28. Y. H. Lee, H. Kim, H. S. Choi, D.-W. Lee and K.-Y. Lee, *Korean J. Chem. Eng.*, **32**, 2220 (2015).
29. X. Du, G. Zou and X. Wang, *Catal. Surv. Asia*, **19**, 17 (2015).
30. C. Matei Ghimbeu, A. Malak-Polaczyk, E. Frackowiak and C. Vix-Guterl, *J. Appl. Electrochem.*, **44**, 123 (2014).
31. H. Chen, J. He, C. Zhang and H. He, *J. Phys. Chem. C.*, **111**, 18033 (2007).
32. M. Jin, J.-N. Park, J. K. Shon, Z. Li, E. Lee and J. M. Kim, *J. Porous Mater.*, **20**, 989 (2013).
33. Y.-T. Wang, A.-H. Lu, H.-L. Zhang and W.-C. Li, *J. Phys. Chem. C.*, **115**, 5413 (2011).
34. W. Yan, T. Ayvazian, J. Kim, Y. Liu, K. C. Donavan, W. Xing, Y. Yang, J. C. Hemminger and R. M. Penner, *ACS Nano*, **5**, 8275 (2011).
35. C.-W. Lee, S.-B. Yoon, S.-M. Bak, J. Han, K. C. Roh and K.-B. Kim, *J. Mater. Chem. A.*, **2**, 3641 (2014).
36. K. Ding, B. Hu, Y. Xie, G. An, R. Tao, H. Zhang and Z. Liu, *J. Mater. Chem.*, **19**, 3725 (2009).
37. M. Zhang, Y. Wu, X. Feng, X. He, L. Chen and Y. Zhang, *J. Mater. Chem.*, **20**, 5835 (2010).
38. H. Lee, S. Kim, D.-W. Lee and K.-Y. Lee, *Catal. Commun.*, **12**, 968 (2011).
39. J. De Laat and H. Gallard, *Environ. Sci. Technol.*, **33**, 2726 (1999).
40. C. P. Huang and Y. H. Huang, *Appl. Catal., A.: Gen.*, **346**, 140 (2008).
41. H. Xia, M. Lai and L. Lu, *J. Mater. Chem.*, **20**, 6896 (2010).
42. B. Soydaş, P. Z. Çulfaz, H. Kalıpçılar and A. Çulfaz, *Cryst. Res. Technol.*, **44**, 800 (2009).
43. G. O. Park, J. K. Shon, Y. H. Kim and J. M. Kim, *J. Nanosci. Nanotechnol.*, **15**, 2441 (2015).
44. G. Leofanti, M. Padovan, G. Tozzola and B. Venturelli, *Catal. Today*, **41**, 207 (1998).